On the relationship between Ural blocking and Arctic-midlatitude thermal gradient

Marco Cadau[1], Gabriele Messori[2,3,4], Marco Gaetani[1], Giorgia Fosser[1], Simona Bordoni[5], Roberto Buizza[6], Gianmaria Sannino [7]

[1]Scuola Universitaria Superiore IUSS, Pavia, Italy
[2]Department of Earth Sciences, Uppsala University, Uppsala, Sweden
[3]Swedish Centre for Impacts of Climate Extremes (climes), Uppsala University, Uppsala, Sweden
[4]Department of Meteorology and Bolin Centre for Climate Research, Stockholm University, Stockholm, Sweden
[5]Department of Civil, Environmental and Mechanical Engineering (DICAM), University of Trento, Trento, Italy
[6]Interdisciplinary Research Center on Sustainability and Climate, Scuola Superiore Sant'Anna, Pisa, Italy
[7]Italian National Agency for New Technologies, Energy and the Environment (ENEA), Rome, Italy

Key Points:

- Ural Blocking can be characterised by strong Arctic-midlatitude thermal gradient
- Co-occurrence of Ural blocking with blocking over Greenland and Chukotka and Urals leads to strong Arctic-midlatitude thermal gradient
- Blocking displacement north of the Ural region leads to weak Arctic-midlatitude thermal gradient

Corresponding author: Marco Cadau, `marco.cadau@iusspavia.it`

Abstract

[In this study, the relationship between the interannual variability of Arctic-midlatitude thermal gradient (AMG) and the winter atmospheric blocking frequency in the Ural region (UBF) is investigated in the ERA5 reanalysis product from 1940 to 2023. In particular, the paper focuses on the large-scale atmospheric circulation patterns associated with high UBF concomitant to weak AMG and vice versa, revisiting the more common and documented relationship connecting intense Ural blocking activity to strong AMG. Results show that displacements of the atmospheric blocking from the Ural region towards the Arctic lead to anomalous southerly thermal advections at polar latitudes and stronger AMG. On the other hand, high blocking frequency co-occurring in the Ural, Greenland and Chukotka regions lead to weaker AMG by limiting northward heat advections towards the Arctic region. These findings highlight a more complex picture of the role of subpolar atmospheric circulation in controlling the AMG.]

Plain Language Summary

[Blocking of the mean atmospheric flow over the Ural region is an important feature of high-latitude weather affecting climate variability in the Arctic. In general, the occurrence of the Ural blocking is associated with warm anomalies in the Arctic, leading to a decrease in the thermal difference between polar and mid latitudes, while reduced blocking activity is generally associated with a larger difference in temperature. This article examines the role of Ural blocking in controlling the Arctic-midlatitudes thermal difference by analyzing unconventional situations. In particular, we find that blocking occurring north of the Ural region leads to a warmer Arctic and a reduced temperature difference, while the co-occurrence of blocking over the Urals, Greenland and Chukotka blocking inhibits the heat transport from mid towards polar latitudes, increasing the thermal difference. These findings contribute to shed light on the mechanisms controlling the Arctic amplification, that is the faster warming of the Arctic region with respect to the global warming.]

1 Introduction

Atmospheric blocking, namely a disruption and/or a deceleration of the mean westerly circumpolar flow, is one of the most important features of the large-scale atmospheric circulation at mid-high latitudes (Davini et al., 2012). Blocking events are associated with anomalous anticyclonic conditions that persist from several days to weeks (Kwon et al., 2020; AMS, American Meteorological Society, 2012; Wazneh et al., 2021). This long persistence is associated with quasi-stationarity (Croci-Maspoli et al., 2007) and self-sustaining or self-preserving mechanisms (Kautz et al., 2022).
During the winter season, the establishment of blocking can lead to large-scale temperature anomalies over the continents in the Northern Hemisphere (NH) and in the Arctic region (Kautz et al., 2022). Winter atmospheric blocking activity in the NH is most frequent in the Bering Strait region, over Greenland and in the Euro-Atlantic sector (1a) (Davini et al., 2012; Woollings et al., 2018; Davini et al., 2021; Hwang et al., 2022). The latter is the most spatially extended blocking region, extending all the way to the Urals. Although Ural blocking (UB) displays a comparatively modest occurrence frequency, it has important repercussions, both locally and in the broader high-latitude Eurasian region. These include affecting sea-ice formation and persistence - especially over the Barents-Kara Seas (Chen et al., 2018; Cho & Kim, 2021) - and influencing Eurasian cooling (Tyrlis et al., 2020; Kim et al., 2022) and Arctic warming (D. Luo, Xiao, Yao, et al., 2016; Yao et al., 2017a). The role of Ural Blocking in inducing these anomalies is modulated by other large-scale patterns, such as the North Atlantic Oscillation and the configuration of the North Atlantic jet (D. Luo, Xiao, Yao, et al., 2016; D. Luo, Xiao, Diao, et al., 2016),

but also by the atmospheric background conditions such as the mean state and vertical shear of the westerly flow (Yao et al., 2017b; D. Luo et al., 2017).
The literature highlights a positive correlation between UB and Arctic temperatures and a negative correlation between UB and Siberian temperatures (D. Luo, Xiao, Yao, et al., 2016; Tyrlis et al., 2020; Papritz, 2020). UB thus acts to reduce the hemispheric-scale temperature gradient. The role of UB in favouring a warmer Arctic has received considerable attention, as one of the several mechanisms potentially modulating Arctic Amplification (AA) (Tyrlis et al., 2020; Cho & Kim, 2021). AA refers to the observed faster-than-global-average warming of the Arctic, which is leading to a decreased thermal gradient between the northern high and mid latitudes (hereafter referred to as Arctic-midlatitude thermal gradient, or AMG) on multidecadal timescales. AA is induced by multiple factors, including (but not limited to) local longwave and shortwave feedbacks, such as lapse rate and sea-ice related feedbacks (Screen & Simmonds, 2010; England et al., 2021), as well as remote influences by poleward energy transport (Graversen & Burtu, 2016; Previdi et al., 2021). The AMG plays an important role in large-scale climate dynamics, by affecting mid-latitude stormtracks (Shaw et al., 2016), meridional moist and dry static energy transports, the orientation and intensity of the jetstream, sea-ice cover and more (Deser et al., 2015; Screen & Francis, 2016).
Notwithstanding the extensive research on AMG and UB, the relationship between the two remains not completely understood. In particular, comparatively little attention has been dedicated to the relationship between the AMG and blocking activity at interannual timescales. This study aims to shed light on this relationship, and verify the extent to which deviations can occur from the expected decreased (increased) gradient in the presence of more (less) UB

2 Data and methods

2.1 Data and significance testing

We use geopotential height at 500 hPa (z500), air temperature at 1000hPa (t1000), meridional wind at 850hPa (v850), the vertical integral of northward total heat flux (HEATF) and of the divergence of thermal energy flux (THERMF) from the ERA5 reanalysis product of the European Centre for Medium-Range Weather Forecasts (Hersbach et al., 2020). All the data are analysed at a 1°x 1°horizontal resolution (remapped from data at a quarter of a degree resolution). Since we focus on large-scale circulation features across the NH, we deem the lower resolution not to affect our analysis. The analysis is performed on 83 boreal winters (December, January and February, DJF), corresponding to 249 months, from December 1940 to February 2023.
Linear correlations are computed using the Pearson correlation coefficient, and considered significant when above the 95% confidence level. The significance of climate variables anomalies is determined using Montecarlo sampling (Kroese et al., 2014) with 5000 iterations, at the 2.5% one-sided significance level.

2.2 Blocking detection

We implement a two-dimensional extension of the Tibaldi and Molteni(Tibaldi & Molteni, 1990) blocking index, introduced by Scherrer et al. (Scherrer et al., 2005). This is amongst the most widely used blocking indices, and is based on the reversal of the meridional gradient of the 500hPa geopotential height (Z500). At each grid point, we compute:

$$GHGN = \frac{(Z500(\lambda, \phi + \delta)) - Z500(\lambda, \phi)}{\delta} \tag{1}$$

$$GHGS = \frac{(Z500(\lambda, \phi)) - Z500(\lambda, \phi - \delta)}{\delta} \tag{2}$$

$$GHGS_2 = \frac{(Z500(\lambda, \phi - \delta)) - Z500(\lambda, \phi - 2\delta)}{\delta} \tag{3}$$

with λ and ϕ indicating longitude and latitude, respectively, and $\delta = 15°$.
In order to consider a grid point as blocked, three conditions must be satisfied:

$$GHGN < -10 \frac{m}{^\circ latitude} \tag{4}$$

$$GHGS > 0 \frac{m}{^\circ latitude} \tag{5}$$

$$GHGS_2 < -5 \frac{m}{^\circ latitude} \tag{6}$$

The first two conditions imply that a blocked area must display a westerly flow on its poleward side (4) and an easterly flow on its equatorward side (5) (Tyrlis et al., 2021). 4 excludes situations when the midlatitude jet is displaced but not blocked, which might be otherwise classified as blocking (Tibaldi & Molteni, 1990). Lastly, 6 excludes cut-off lows and subtropical features (Davini et al., 2012; Woollings et al., 2018).
In this study, we only consider instantaneous blocking (IB) (Davini et al., 2012; Davini & D'Andrea, 2020), namely not implementing any temporal persistence condition or spatial extent constraint. We define UB as IB occurring in the Ural region [54°-64°N, 48°-67°E] (highlighted in yellow in Figure 1a). A Ural Blocking Index (UBI) is then calculated as follows. We first determine the monthly blocking frequency at each gridpoint as the percentage of days with presence of blocking over the total of the days of the month. We next compute an area-weighted spatial average, across all gridpoints within the selected Ural region.

2.3 Arctic-midlatitudes thermal gradient

The AMG definition is based on the 1000hPa temperature anomalies, following Francis and Vavrus, 2015 and Davy et al., 2018 (Francis & Vavrus, 2015; Davy et al., 2018). We subtract the monthly temperature anomaly of the [30-60°N] band from the corresponding anomaly of the [70-90°N] band. The anomalies are computed with respect to the corresponding monthly long term climatology. For example, the t1000 anomaly for December 1940 is given by the difference in temperature, previously averaged over the selected latitude band, between December 1940 and the areal mean climatological temperature for all Decembers over the 1940-2022 period. Thus, high values of the AMG index are associated with a lower than average meridional gradient, and viceversa.
The resulting AMG timeseries (Figure 1b) includes both high frequency and low frequency variability. The long-term increasing trend is the footprint of AA, and corresponds to a faster warming of the high latitude band compared to the midlatitudes. A visual inspection nonetheless suggests that the increasing trend is non-monotonic. In order to isolate the high-frequency (HF) component of the signal, the low frequency component, estimated by applying a 6th grade polynomial fit, is subtracted from the AMG time series. The HF component is isolated from each month (D, J and F) separately. The resulting AMG-HF is displayed in the supplementary material (Figure **??**). The application of a low-pass filter with a cut-off frequency of 8 years leads to similar results (not shown), indicating that the definition of the HF component of the AMG is not sensitive to the filtering method.
We interpret AMG-HF as illustrating the AA's interannual variability.

3 Results

In agreement with previous research, we find a significant positive correlation between UB frequency and AMG (Figure 1c). Indeed, the Urals are the blocking region displaying the strongest absolute correlation values. Thus, Ural blockings are more frequent in months characterised by a positive AMG index (associated to a reduced meridional thermal gradient), and viceversa.

A similar, but stronger, signal is found when the long-term variability is removed to AMG (Figure 1d). This suggests that the UB relationship is stronger at the interannual time scale. Specifically, the correlation coefficient spatially averaged over the Ural

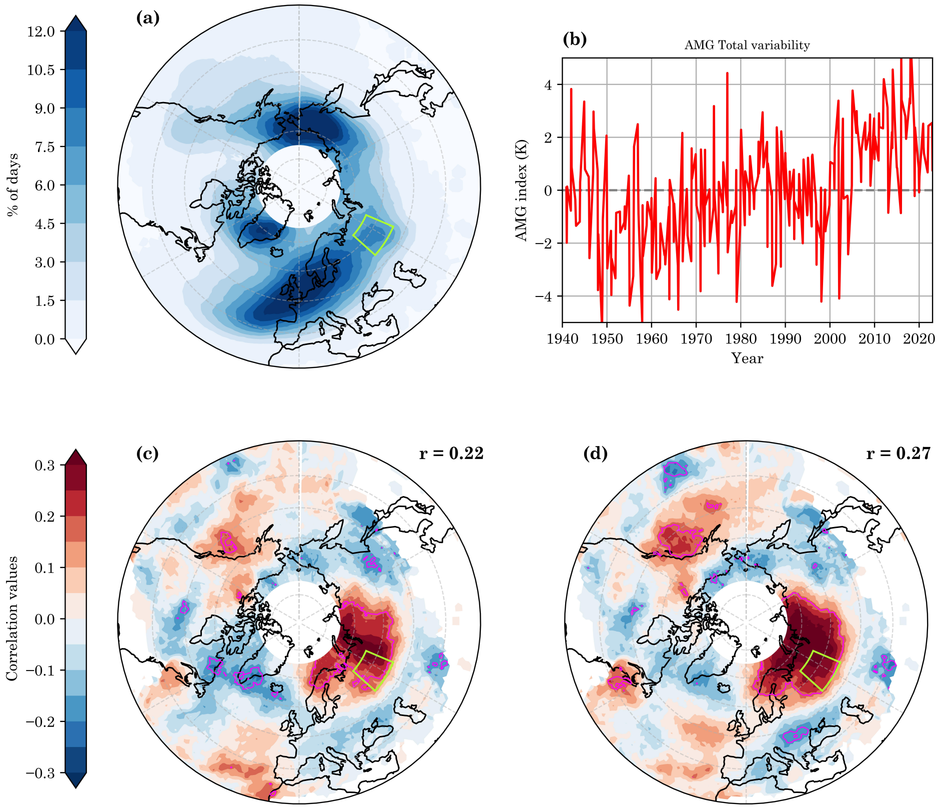

Figure 1. (a) DJF Climatology of instantaneous blocking (IB) frequency in the [30-75°N] band. The Ural region is highighted by the light green box. (b) Arctic-midlatitudes thermal gradient (AMG), DJF monthly means from 1940 to 2022. Note that timeseries ony displays DJF values for each year. Pearson correlation maps between monthly timeseries of IB and AMG: (c) unfiltered and (d) high frequency. Magenta lines mark significance at the 5% level. In panels (c) and (d), the correlation coefficients spatially averaged over the Ural region (light green box), with their p-values, are displayed. Correlation coefficients spatial averages are statistically significant at the 1% level.

region expresses about 7.2% of the shared variability for the AMG-HF, against less than 5% for the raw AMG index. We thus focus on the relationship between AMG-HF and UBI.

As expected from the correlation map, the months with high Ural blocking activity are likely to be months with large AMG-HF index values, and the converse. However, there are also relatively numerous cases where high Ural blocking activity coincides with a low AMG-HF index and viceversa. This is not entirely unexpected, as the linear correlation explains a relatively small fraction of the covariance between the two variables.

To better characterize these ”unconventional” cases, in Figure 2, we classify all the 249 DJF months we analyse according to their joint AMG-HF and instantaneous Ural Blocking values. We select four subsets of months for further analysis: two are the ”conventional” cases of high (low) AMG-HF index values and strong (weak) UBI, including 36 (51) months. We hereafter name this case SS (WW), from Strong AMG-HF-Strong UBI (WW, from Weak AMG-HF-Weak UBI). Part of the remaining months fall into the unconventional cases of low (high) AMG-HF index and strong (weak) Ural blocking, in-

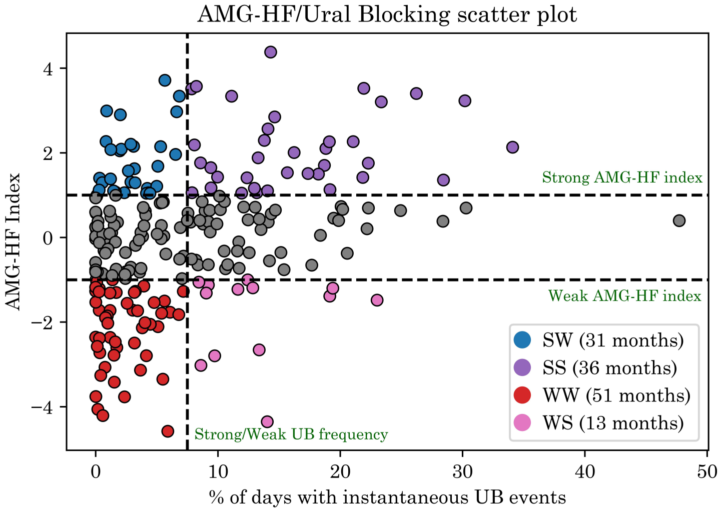

Figure 2. Scatterplot of monthly UBI and AMG-HF index. Blue dots display anomalously positive AMG-HF index values associated with low UBI (strong AMG-HF index and weak UBI, SW). Purple dots display anomalously high AMG-HF index values associated with high UBI (strong AMG-HF index and strong UBI, SS). Red dots display anomalously negative AMG-HF index values associated with low UBI (weak AMG-HF index and weak UBI, WW). Pink dots display anomalously negative AMG-HF index values associated with high UBI (weak AMG-HF index and strong UBI, SS). The sample sizes of the WW, WS, SW and SS are indicated in the legend.

cluding 13 (31) months, hereafter named WS (SW). Note that high (low) values of the AMG-HF index are associated with a gradient weaker (stronger) than usual.
To define these four sets of months, we use thresholds values of ± 1 K for the AMG-HF index, approximately corresponding to the 25th and 75th percentiles of the index. We further use a cutoff of 7.5% blocking frequency to separate strong and weak UBI, approximately corresponding to the 61st percentile of the UBI distribution.

To shed light on the dynamical features of the AMG-UB relationship at the interannual time scale, the large-scale atmospheric circulation patterns associated with the identified classes of events are analysed.
When both the AMG-HF index and UBI are lower than usual (WW case) we observe a significant decrease in frequency of IB from Scandinavia through Eastern Europe and across Siberia (Figure 3a). Hence, the observed decreased blocking frequency signal is not limited to Urals, but extended to a much broader region. An analogous decrease is observed in the Gulf of Alaska and, at the same time, blocking frequency increases in Southeastern Europe. Z500 anomalies reflect the blocking anomalies (Figure 3a). The t1000 patterns are characterized by widespread negative anomalies over the Arctic region, and an extended positive anomaly over Eurasia (Figure 3b). The decreased UB frequency further shows its signature in meridional 850 hPa wind (Figure 3c) which displays a cyclonic anomaly over the Ural region. A positive anomaly over Northern Canada is observed, as well as a negative v850 anomaly south of Greenland and in the North Atlantic region south of the Arctic ocean. The latter suggests a weakened advection of warm and moist airmasses towards the polar latitudes from the North Atlantic sector, contributing to the higher-than-average meridional temperature gradient. This interpretation is supported by the HEATF anomalies (Figure **??**a), strongly resembling the spatial pattern of v850. Finally, the area-weighted spatial average of the THERMF anomalies over

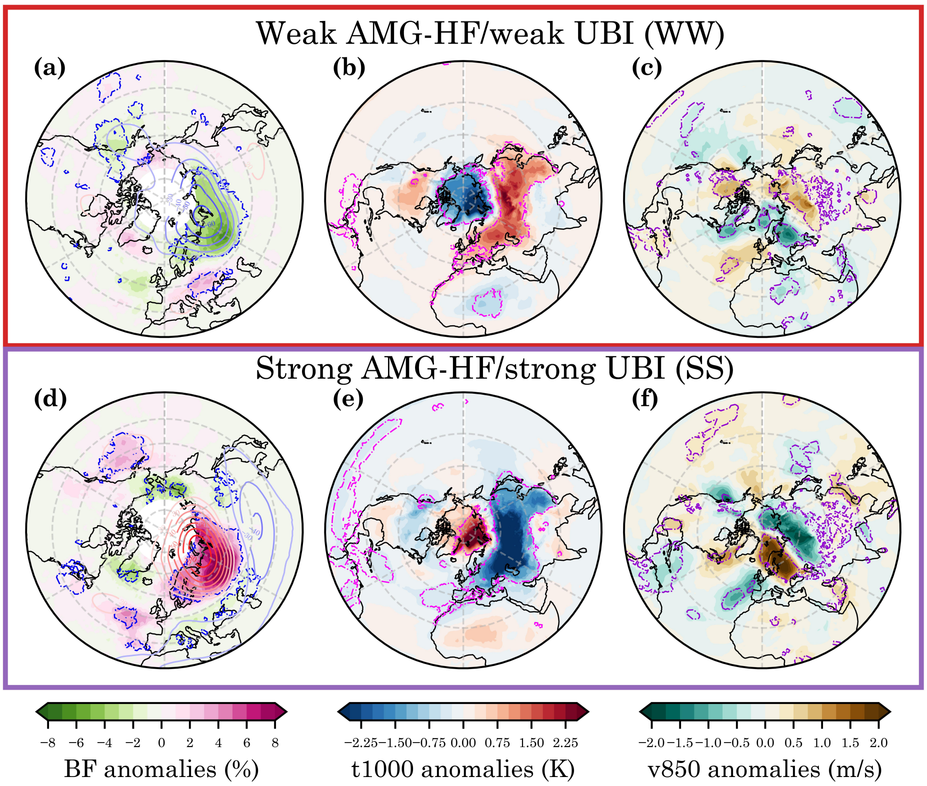

Figure 3. Compound climate anomalies for the four sets of months defined in 3 and in Figure 2: low AMG-HF index/weak UB (red), high AMG-HF index/strong UB (purple), high AMG-HF index/weak UB (blue) and low AMG-HF index/strong UB (pink). Anomalies are shown for the following variables: (a), and (d) Blocking Frequency (BF); (b) and (e) 1000hPa temperature; (c) and (f) 850hPa meridional wind. Dashed contours denote significant anomalies at the 95% confidence level, determined using Monte Carlo sampling with 5000 iterations. blue-to-red scale contours on BF anomalies represent 500hPa geopotential anomalies for the same time frame.

the Arctic region (defined as for the AMG metric, as the [70-90°N] band) is positive (8.85 W/m) in the WW case: positive values of this indicator are associated with a net divergence of the thermal energy flux over the Arctic. gradient.

When both AMG-HF index and Ural Blocking activity are higher than usual (SS), the anomalies are approximately symmetric to the WW case (Figure 3d-f). The main differences are a significant negative anomaly in blocking frequency over southern Greenland and a positive anomaly over the North Atlantic. The THERMF pattern is also consistent with the previous interpretation of the WW case, since the Arctic THERMF spatial average is statistically significantly negative at -18.76 W/m, suggesting a net convergence of thermal energy flux in the Arctic.

We next consider the two unconventional cases in the relationship between Ural Blocking and AMG. The SW case displays negative IB frequency anomalies over the Urals (Figure 4a). However, unlike the WW case (Figure 3a), the region of negative anomalies is much more spatially confined. A positive signal over the Barents-Kara seas suggest that the weakening of the UB reflects a northward shift of the blocking region, which cannot be captured by our blocking metric, defined south of 75°N. Nevertheless, the hypothesis of a displacement of the blocking regions is supported by the positive z500 anomalies seen over the Arctic Ocean (Figure 4a). T1000 anomalies are strongly positive over

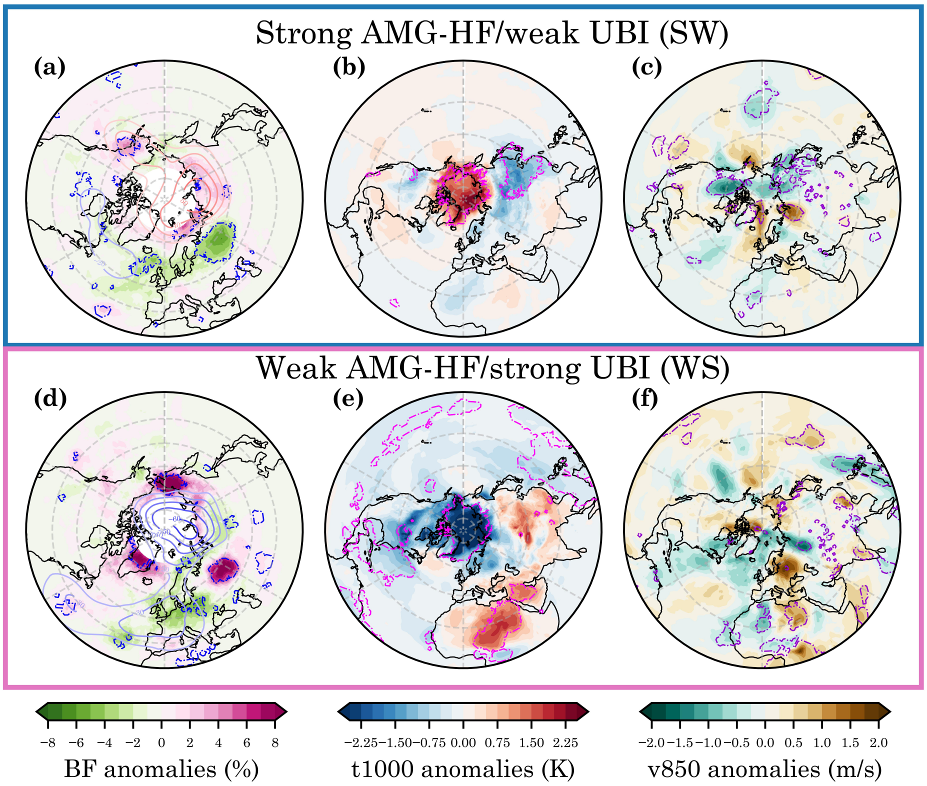

Figure 4. Same as in 3, but for (a-c) SW and (d-f) WS.

the Arctic. They are however widespread across the Arctic basin, unlike for the SS case, where the strongest positive anomalies were concentrated in the Barents-Kara seas region (cf. Figure 4b, Figure 3e). The negative anomalies over Eurasia are weak, and confined to Eastern Siberia. V850 anomalies show a cyclonic pattern anomaly over Siberia, a strong negative anomaly over central Canada and positive anomalies in the North Atlantic sector. This latter, along with the HEATF anomalies pattern (Figure **??**a) suggests enhanced advection of midlatitude airmasses towards the high latitudes.

The WS case shows anomalies which only partly mirror those for the SW case. The positive UBI anomaly is intense, but geographically very localized (Figure 4d). Strong positive blocking anomalies are also found in correspondence with the climatological maxima in Greenland and the Bering Strait. These anomalies exceed 6%, namely over 50% of the climatological values (Figure 1a) of about 8-12% of blocking days. The Z500 anomalies are strongly negative in the Arctic basin, but unlike the SW case, do not form an Arctic-mid latitude dipole (Figure 4d). The t1000 pattern displays a colder-than-average Arctic, similar to the WW case, yet with stronger and more widespread negative anomalies (cf. Figure 3b, Figure 4e). Moreover, there is only a weak warming signal over Eurasia, with the cold anomalies extending from the Arctic into Scandinavia, Western Russia and northern North America. Both positive and negative temperature anomalies are found across the lower midlatitudes: in particular, a significant and positive temperature anomaly is present over central Sahara and over the Arabian desert. Finally, the v850 anomalies do not display relevant significant signals, apart from the anticyclonic pattern over the Ural region, albeit less marked than for SS (cf. Figure 4f, Figure 3f). Although not significant, a negative anomaly over the North Atlantic might suggest, as in the SW case, a weakened heat and moisture transport towards the polar latitudes, as also supported by the HEATF anomalies showing again a strong association between merid-

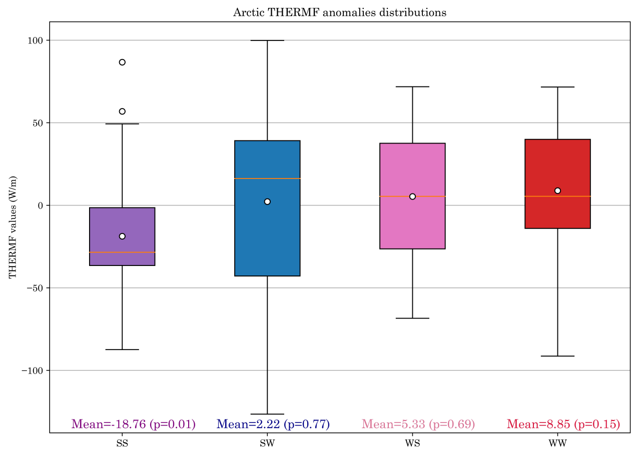

Figure 5. Box plot of the THERMF anomalies over the Arctic region (North of 70°N). Means are highlighted in white, and their numerical values are displayed at the bottom of the figure. P-values (in parentheses) are derived from bootstrap resampling with 5000 iterations.

ional wind and heat transport (for both the unconventional cases) (Figure **??**a,d). The Arctic spatial averages of the THERMF anomalies are not significantly different from zero for both latter cases.
Focusing on the THERMF anomalies of the different cases, we note that they increase from SS to SW, WS and WW (Figure 5). Specifically, conventional cases with a strong (weak) AMG-HF index show net convergence (divergence), on average, in the Arctic. For WS, a nearly-zero anomaly value is linked with the fact that blocking co-occurrence in multiple high-latitude areas effectively inhibits meridional energy transport from the lower latitudes.

4 Discussion and Conclusions

In this study, we analysed the relationship between Ural Blocking and the Arctic-Midlatitude thermal gradient. We found that Ural Blocking positively correlates with the AMG on interannual timescales. Specifically, when Ural Blocking is suppressed, we observe negative geopotential height anomalies over the Arctic and Siberia and positive anomalies in the midlatitudes. This is associated with an anomalous cyclonic circulation over the Ural region and reduced advection of midlatitude air to the Arctic, resulting in a colder Arctic, a warmer Eurasia, and an anomalously large meridional temperature gradient. Conversely, when Ural Blocking is enhanced, there are positive Z500 anomalies over Siberia and negative anomalies further South, an anticyclonic circulation anomaly over the Urals, and enhanced advection of midlatitude airmasses towards the Arctic. This results in an anomalously warm Eurasian Arctic, and an anomalously cold Eurasia. These findings are in line with the known role of Ural blocking in modulating Arctic temperatures and sea-ice cover, and with the Warm Arctic - Cold Eurasia pattern which has been amply discussed in the literature (D. Luo, Xiao, Yao, et al., 2016; D. Luo, Xiao, Diao, et al., 2016; Tyrlis et al., 2020; Ye & Messori, 2020).
However, the linear correlation between Ural Blocking and the meridional temperature gradient only explains a small amount of the shared variability, indicating that a more complex relationship is in place. Therefore, we explored the Ural Blocking – Arctic-Midlatitude thermal gradient connection focusing on the situations characterised by intense Ural blocking activity and strong gradient, and viceversa. When reduced Ural blocking activity is accompanied by a weaker gradient, we show that the reduced blocking is actually the consequence of a northward shift of the blocking area, from the Ural region to the Barents-

Kara seas. This is associated with positive Z500 anomalies over the Arctic basin, and a spatially extended positive temperature anomaly in the Arctic ocean. Eurasian cold temperature anomalies are relatively weak, suggesting that the warm anomalies in the Arctic, associated with the blocking displacement, are the main drivers of the reduced meridional temperature gradient. On the other hand, when intense Ural Blocking is accompanied by a stronger gradient, we observe blocking developing more frequently than climatology over Greenland and close to the Bering Strait region, hindering poleward advection of midlatitude airmasses and resulting in a colder than usual Arctic. Associated with the concomitant occurrence of Ural, Greenland and Bering Strait region blocking, widespread anomalies are observed over northern Africa. These may originate from the interplay between the blocking anomalies and jet dynamics or hemispheric Rossby-wave patterns. Again, the Arctic anomalies appear as the main drivers of the anomalous meridional temperature gradient.
Our results show that the documented relationship between UB and Arctic thermal anomalies can be modulated by modifications in the large-scale circulation in the NH at the interannual time scale. In particular, a displacement of the Ural Blocking area or the concomitant occurrence of blocking over Greenland and the Bering Strait may drive warm or cold anomalies in the Arctic, respectively.
Ultimately, our analysis can be useful for a better comprehension of the relationship between Ural Blocking and other mid-high latitude climate features already investigated in literature, such as Arctic sea ice and Barents-Kara Seas atmospheric dynamics (Ruggieri et al., 2016, 2017; Chen et al., 2018; Ahmadi & Alizadeh, 2023), the stratospheric polar vortex (Peings, 2019; Tyrlis et al., 2019), and atmospheric variability modes such as North Atlantic Oscillation (B. Luo et al., 2021; Ahmadi & Alizadeh, 2023; Peings et al., 2023).

5 Data Availability Statement

All underlying ERA5 reanalysis datasets are publicly available from the Copernicus Climate Data Store: `https://cds.climate.copernicus.eu/cdsapp#!/home`. Python scripts implemented for this work are available upon request.

Acknowledgments
This paper and related research have been conducted during and with the support of the Italian inter-university PhD course in sustainable development and climate change (link: www.phd-sdc.it).
MG acknowledge the support of the project "Dipartimento di Eccellenza 2023–2027", funded by the Italian Ministry of Education, University and Research at IUSS Pavia.
GM has received funding from the European Union's H2020 research and innovation programme under ERC grant no. 948309 (CENÆ project).
SB acknowledges partial support from the National Recovery and Resilience Plan (NRRP), Mission 4 Component 2 Investment 1.4 - Call for tender No. 1031 of 17/06/2022 of Italian Ministry for University and Research funded by the European Union – NextGenerationEU (proj. nr. CN_00000013)

References

Ahmadi, R., & Alizadeh, O. (2023, 8). The possible links between the barents–kara sea-ice area, ural blocking, and the north atlantic oscillation. *Quarterly Journal of the Royal Meteorological Society*. doi: 10.1002/qj.4560

AMS, American Meteorological Society. (2012). *Blocking.* Retrieved from `https://glossary.ametsoc.org/wiki/Blocking`

Chen, X., Luo, D., Feldstein, S. B., & Lee, S. (2018, 3). Impact of winter ural blocking on arctic sea ice: Short-time variability. *Journal of Climate*, *31*, 2267-2282.

doi: 10.1175/JCLI-D-17-0194.1
Cho, D.-J., & Kim, K.-Y. (2021, 3). Role of ural blocking in arctic sea ice loss and its connection with arctic warming in winter. *Climate Dynamics*, *56*, 1571-1588. doi: 10.1007/s00382-020-05545-3
Croci-Maspoli, M., Schwierz, C., & Davies, H. C. (2007, 2). A multifaceted climatology of atmospheric blocking and its recent linear trend. *Journal of Climate*, *20*, 633-649. doi: 10.1175/JCLI4029.1
Davini, P., Cagnazzo, C., Gualdi, S., & Navarra, A. (2012, 10). Bidimensional diagnostics, variability, and trends of northern hemisphere blocking. *Journal of Climate*, *25*, 6496-6509. doi: 10.1175/JCLI-D-12-00032.1
Davini, P., & D'Andrea, F. (2020, 12). From cmip3 to cmip6: Northern hemisphere atmospheric blocking simulation in present and future climate. *Journal of Climate*, *33*, 10021-10038. doi: 10.1175/JCLI-D-19-0862.1
Davini, P., Weisheimer, A., Balmaseda, M., Johnson, S. J., Molteni, F., Roberts, C. D., … Stockdale, T. N. (2021, 1). The representation of winter northern hemisphere atmospheric blocking in ecmwf seasonal prediction systems. *Quarterly Journal of the Royal Meteorological Society*, *147*, 1344-1363. doi: 10.1002/qj.3974
Davy, R., Chen, L., & Hanna, E. (2018, 10). Arctic amplification metrics. *International Journal of Climatology*, *38*, 4384-4394. doi: 10.1002/joc.5675
Deser, C., Tomas, R. A., & Sun, L. (2015, 3). The role of ocean–atmosphere coupling in the zonal-mean atmospheric response to arctic sea ice loss. *Journal of Climate*, *28*, 2168-2186. doi: 10.1175/JCLI-D-14-00325.1
England, M. R., Eisenman, I., Lutsko, N. J., & Wagner, T. J. W. (2021, 8). The recent emergence of arctic amplification. *Geophysical Research Letters*, *48*. doi: 10.1029/2021GL094086
Francis, J. A., & Vavrus, S. J. (2015, 1). Evidence for a wavier jet stream in response to rapid arctic warming. *Environmental Research Letters*, *10*, 014005. doi: 10.1088/1748-9326/10/1/014005
Graversen, R. G., & Burtu, M. (2016, 7). Arctic amplification enhanced by latent energy transport of atmospheric planetary waves. *Quarterly Journal of the Royal Meteorological Society*, *142*, 2046-2054. doi: 10.1002/qj.2802
Hersbach, H., Bell, B., Berrisford, P., Hirahara, S., Horányi, A., Muñoz-Sabater, J., … Thépaut, J. (2020, 7). The era5 global reanalysis. *Quarterly Journal of the Royal Meteorological Society*, *146*, 1999-2049. doi: 10.1002/qj.3803
Hwang, J., Son, S.-W., Martineau, P., & Barriopedro, D. (2022, 10). Impact of winter blocking on surface air temperature in east asia: Ural versus okhotsk blocking. *Climate Dynamics*, *59*, 2197-2212. doi: 10.1007/s00382-022-06204-5
Kautz, L.-A., Martius, O., Pfahl, S., Pinto, J. G., Ramos, A. M., Sousa, P. M., & Woollings, T. (2022, 3). Atmospheric blocking and weather extremes over the euro-atlantic sector – a review. *Weather and Climate Dynamics*, *3*, 305-336. doi: 10.5194/wcd-3-305-2022
Kim, S.-H., Sung, H.-J., Kim, S.-J., Baek, E.-H., Moon, J.-Y., & Kim, B.-M. (2022, 7). Contribution of ural and kamchatka blockings to the amplified warm arctic–cold eurasia pattern under arctic sea ice loss and eurasian cooling. *Journal of Climate*, *35*, 4071-4083. doi: 10.1175/JCLI-D-21-0635.1
Kroese, D. P., Brereton, T., Taimre, T., & Botev, Z. I. (2014, 11). Why the monte carlo method is so important today. *WIREs Computational Statistics*, *6*, 386-392. doi: 10.1002/wics.1314
Kwon, Y.-O., Seo, H., Ummenhofer, C. C., & Joyce, T. M. (2020, 2). Impact of multidecadal variability in atlantic sst on winter atmospheric blocking. *Journal of Climate*, *33*, 867-892. doi: 10.1175/JCLI-D-19-0324.1
Luo, B., Luo, D., Dai, A., Simmonds, I., & Wu, L. (2021, 9). A connection of winter eurasian cold anomaly to the modulation of ural blocking by enso. *Geophysical Research Letters*, *48*. doi: 10.1029/2021GL094304

Luo, D., Xiao, Y., Diao, Y., Dai, A., Franzke, C. L. E., & Simmonds, I. (2016, 6). Impact of ural blocking on winter warm arctic–cold eurasian anomalies. part ii: The link to the north atlantic oscillation. *Journal of Climate*, *29*, 3949-3971. doi: 10.1175/JCLI-D-15-0612.1

Luo, D., Xiao, Y., Yao, Y., Dai, A., Simmonds, I., & Franzke, C. L. E. (2016, 6). Impact of ural blocking on winter warm arctic–cold eurasian anomalies. part i: Blocking-induced amplification. *Journal of Climate*, *29*, 3925-3947. doi: 10.1175/JCLI-D-15-0611.1

Luo, D., Yao, Y., Dai, A., Simmonds, I., & Zhong, L. (2017, 5). Increased quasi stationarity and persistence of winter ural blocking and eurasian extreme cold events in response to arctic warming. part ii: A theoretical explanation. *Journal of Climate*, *30*, 3569-3587. doi: 10.1175/JCLI-D-16-0262.1

Papritz, L. (2020, 2). Arctic lower-tropospheric warm and cold extremes: Horizontal and vertical transport, diabatic processes, and linkage to synoptic circulation features. *Journal of Climate*, *33*, 993-1016. doi: 10.1175/JCLI-D-19-0638.1

Peings, Y. (2019, 5). Ural blocking as a driver of early-winter stratospheric warmings. *Geophysical Research Letters*, *46*, 5460-5468. doi: 10.1029/2019GL082097

Peings, Y., Davini, P., & Magnusdottir, G. (2023, 3). Impact of ural blocking on early winter climate variability under different barents-kara sea ice conditions. *Journal of Geophysical Research: Atmospheres*, *128*. doi: 10.1029/2022JD036994

Previdi, M., Smith, K. L., & Polvani, L. M. (2021, 9). Arctic amplification of climate change: a review of underlying mechanisms. *Environmental Research Letters*, *16*, 093003. doi: 10.1088/1748-9326/ac1c29

Ruggieri, P., Buizza, R., & Visconti, G. (2016, 5). On the link between barents-kara sea ice variability and european blocking. *Journal of Geophysical Research: Atmospheres*, *121*, 5664-5679. doi: 10.1002/2015JD024021

Ruggieri, P., Kucharski, F., Buizza, R., & Ambaum, M. H. P. (2017, 4). The transient atmospheric response to a reduction of sea-ice cover in the barents and kara seas. *Quarterly Journal of the Royal Meteorological Society*, *143*, 1632-1640. doi: 10.1002/qj.3034

Scherrer, S. C., Croci-Maspoli, M., Schwierz, C., & Appenzeller, C. (2005, 2). Two-dimensional indices of atmospheric blocking and their statistical relationship with winter climate patterns in the euro-atlantic region. *International Journal of Climatology*, *26*, 233-249. doi: 10.1002/joc.1250

Screen, J. A., & Francis, J. A. (2016, 9). Contribution of sea-ice loss to arctic amplification is regulated by pacific ocean decadal variability. *Nature Climate Change*, *6*, 856-860. doi: 10.1038/nclimate3011

Screen, J. A., & Simmonds, I. (2010, 4). The central role of diminishing sea ice in recent arctic temperature amplification. *Nature*, *464*, 1334-1337. doi: 10.1038/nature09051

Shaw, T. A., Baldwin, M., Barnes, E. A., Caballero, R., Garfinkel, C. I., Hwang, Y.-T., . . . Voigt, A. (2016, 9). Storm track processes and the opposing influences of climate change. *Nature Geoscience*, *9*, 656-664. doi: 10.1038/ngeo2783

Tibaldi, S., & Molteni, F. (1990). On the operational predictability of blocking. *Tellus A*, *42*, 343-365. doi: 10.1034/j.1600-0870.1990.t01-2-00003.x

Tyrlis, E., Bader, J., Manzini, E., & Matei, D. (2021, 1). Reconciling different methods of high-latitude blocking detection. *Quarterly Journal of the Royal Meteorological Society*, *147*, 1070-1096. Retrieved from `https://onlinelibrary.wiley.com/doi/10.1002/qj.3960` doi: 10.1002/qj.3960

Tyrlis, E., Bader, J., Manzini, E., Ukita, J., Nakamura, H., & Matei, D. (2020, 7). On the role of ural blocking in driving the warm arctic–cold siberia pattern. *Quarterly Journal of the Royal Meteorological Society*, *146*, 2138-2153. doi: 10.1002/qj.3784

Tyrlis, E., Manzini, E., Bader, J., Ukita, J., Nakamura, H., & Matei, D. (2019, 11). Ural blocking driving extreme arctic sea ice loss, cold eurasia, and stratospheric vortex weakening in autumn and early winter 2016–2017. *Journal of Geophysical Research: Atmospheres*, *124*, 11313-11329. doi: 10.1029/2019JD031085

Wazneh, H., Gachon, P., Laprise, R., de Vernal, A., & Tremblay, B. (2021, 4). Atmospheric blocking events in the north atlantic: trends and links to climate anomalies and teleconnections. *Climate Dynamics*, *56*, 2199-2221. Retrieved from `https://link.springer.com/10.1007/s00382-020-05583-x` doi: 10.1007/s00382-020-05583-x

Woollings, T., Barriopedro, D., Methven, J., Son, S. W., Martius, O., Harvey, B., ... Seneviratne, S. (2018). Blocking and its response to climate change. *Current Climate Change Reports*, *4*, 287-300. doi: 10.1007/s40641-018-0108-z

Yao, Y., Luo, D., Dai, A., & Simmonds, I. (2017a, 5). Increased quasi stationarity and persistence of winter ural blocking and eurasian extreme cold events in response to arctic warming. part i: Insights from observational analyses. *Journal of Climate*, *30*, 3549-3568. doi: 10.1175/JCLI-D-16-0261.1

Yao, Y., Luo, D., Dai, A., & Simmonds, I. (2017b, 5). Increased quasi stationarity and persistence of winter ural blocking and eurasian extreme cold events in response to arctic warming. part i: Insights from observational analyses. *Journal of Climate*, *30*, 3549-3568. doi: 10.1175/JCLI-D-16-0261.1

Ye, K., & Messori, G. (2020, 7). Two leading modes of wintertime atmospheric circulation drive the recent warm arctic–cold eurasia temperature pattern. *Journal of Climate*, *33*, 5565-5587. doi: 10.1175/JCLI-D-19-0403.1